The Barostrat Instability: the baroclinic instability in a rotating stratified fluid

Patrice Le Gal[1], Miklos Vincze[2], Ion Borcia[3], Uwe Harlander[3]

[1]IRPHE, CNRS - Aix Marseille University - Centrale Marseille, 49 rue F. Joliot Curie, 13384 Marseille Cedex 13, France. legal@irphe.univ-mrs.fr
[2]MTA-ELTE Theoretical Physics Research Group, Pazmany P. stny. 1/a. H-1117, Budapest, Hungary
[3]Lehrstuhl Aerodynamik und Strmungsmechanik, Brandenburgische Technische Universitt Cottbus-Senftenberg, Siemens-Halske-Ring 14, 03046 Cottbus, Germany

Abstract

Our project aims to describe the baroclinic instability that destabilizes an initially stratified layer of fluid. Classically, this instability is studied using pure fluid. Here, the originality of our experiment comes from the use of a layer of water initially stratified with salt. Before rotation is started, double convection sets in within the stratified layer with a strongly nonhomogeneous pattern consisting of a double diffusive staircase at the bottom of the container in the very dense water layer and a shallow convective cell in the top surface layer. These two layers are separated by a motionless stably stratified zone. As radial motions take place due to the presence of these convective cells, the action of the Coriolis force generates strong zonal flows as soon as rotation is started. Then, above a rotation rate threshold, the baroclinic instability destabilizes the flow in the top shallow convective layer, generating a ring of pancake vortices sitting above the stably stratified layer. Therefore, this laboratory arrangement mimics the presence of a stratosphere above a baroclinic unstable troposphere. Infrared camera images measure the temperature distributions at the water surface and PIV velocity maps describe the wavy flow pattern at different altitudes. In some regimes, some wave trains have been detected. These waves might be traces of Internal Gravity Waves generated by the fluid motions in the baroclinic unstable layer.

1 Introduction

The differentially heated rotating annulus is a widely studied experimental apparatus for modeling large-scale features of the mid-latitude atmosphere (planetary waves, cyclogenesis). In the classic set-up, a rotating cylindrical tank is divided into three coaxial sections: the innermost domain is kept at a lower temperature, whereas the outer rim of the tank is heated. The working fluid in the annular gap in between thus experiences a radial temperature difference. These boundary conditions imitate the meridional temperature gradient of the terrestrial (or more generally planetary) atmosphere between the poles and the equator. The Coriolis effect arising due to the rotation of the tank modifies this convective pattern and yields a strong zonal flow with directions alternating with depth. Then at large enough values of the rotation rate, this azimuthaly symmetric basic flow becomes unstable and leads to the well known baroclinic instability with the formation of cyclonic and anticyclonic eddies in the full water depth. In the present work, we study a modified version of this experiment, in which besides the aforementioned radial temperature difference a vertical salinity stratification characterized by a buoyancy frequency N is also present. Whereas the baroclinic instability experiments are classical models of mid-latitude atmospheric dynamics, our aim here is to create a juxtaposition of convective

and motionless stratified layers in the laboratory. We expect therefore that our original experimental arrangement can mimic the convective and radiative zones of stars, the tropospheres and stratospheres of planetary atmospheres or the surface turbulent sea layers above deeper stratified waters. Let us stress in particular that the exchange of momentum and energy between these layers (by the propagation of internal gravity waves for instance) is a major issue in astrophysics and geophysical sciences, in particular for the parametrization of subgrid hydrodynamics scales of forecast models. Therefore, we claim that our present set-up may lead to new insights in geo- and astrophysical applications.

2 Experimental set-up and methods

The experiments of the present study were conducted in the laboratory set-up sketched in Fig. 1. The working fluid consists of sodium-chloride/de-ionized water solution, with Lewis number $Le \equiv \kappa_T/\kappa_S \approx 100$, where κ_T and κ_S are the diffusion coefficients for heat and salt, respectively. The radii of the inner (cooling) and outer (heating) cylinders were $a = 4.5$ cm and $b = 12$ cm, yielding a $d = b - a = 7.5$ cm wide annular cavity that was filled up to heights ranging from $D = 10$ cm to $D = 13$ cm in the different runs. In the experimental runs discussed here, the lateral temperature difference ΔT was set between 4 K and 10 K, and a continuously stratified salinity profile with a buoyancy frequency 1 rad/s $<$ N $<$ 5 rad/s, was initially prepared in the annular cavity with the standard double-bucket technique.

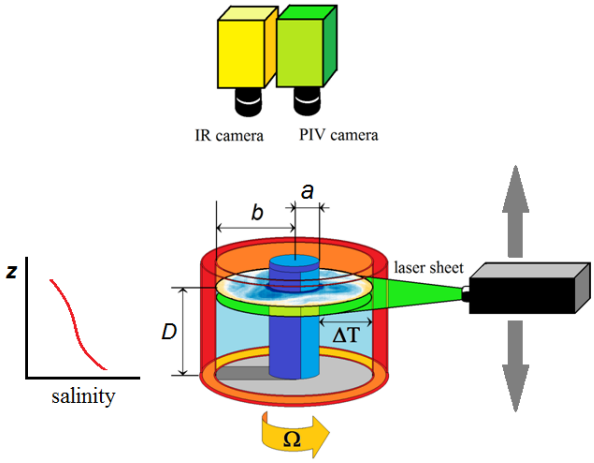

Figure 1: A schematic drawing of the experimental set-up, with parameters $a = 4.5$ cm, $b = 12$ cm, $D = 10 - 13$ cm, $\Omega = 1.7 - 2.7$ rpm, $\Delta T = 6K$. The direction of the tank's rotation is also indicated.

Large enough stable vertical salinity gradients may inhibit the formation of full-depth (unicellular) overturning flow, even in such laterally heated systems as the rotating annulus experiments. The vertical extent of a convective cell is naturally limited by the condition that the initial (saline) density difference between the top and bottom of the cell cannot exceed the (thermal) horizontal density difference between the lateral sidewalls, i.e.:

$$\langle\rho\rangle\alpha\Delta T \approx \lambda\left|\frac{\partial\rho}{\partial z}\right|, \tag{1}$$

where $\langle\rho\rangle$ is the average density within the cell, α the coefficient of thermal expansion

and λ the characteristic vertical (direction z) extent of the convective cell. This scale can be expressed using the buoyancy frequency $N(z) = \sqrt{g\langle\rho(z)\rangle^{-1}\,|d\rho(z)/dz|}$, in the form:

$$\lambda(z) = \frac{g\alpha\Delta T}{N^2(z)}. \tag{2}$$

This characteristic vertical scale of *double-diffusive convection* is referred to as the Chen scale, since the pioneering experimental analysis of Chen et al. (1971). Within each cell, the convective flow yields mixing and the initial stratification vanishes. Thus, a so-called "double-diffusive staircase" can develop with jump-wise density changes between these locally homogenized cells. Even before starting rotation, the onset of double diffusive convection can be observed visually in experiments. Generally, most of our prepared vertical profiles yielded conditions where convection in the bulk is mostly inhibited. However, the no-flux conditions for salinity at the bottom and the top of the water body translate to $N \approx 0$ conditions at these regions in terms of buoyancy frequency. Thus in thin layers at the vicinity of these boundaries where $N < N_{\text{crit}}$ holds, localized convective cells could still invade the water layer on a depth $\approx \lambda$, as seen in Fig. 2. Note that the stratified zone will be gently eroded in time, but it is worth noting that we can keep the confinement of convection for several days before complete mixing of salt water.

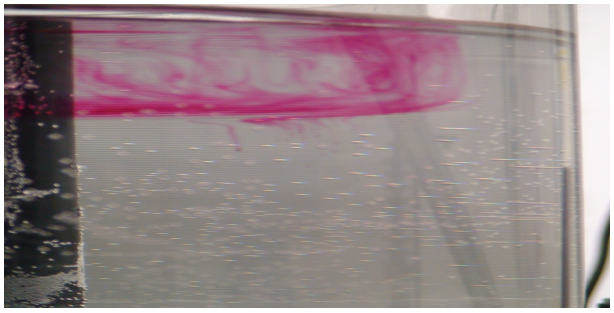

Figure 2: A snapshot of the double diffusive cell at the top of the experimental tank during a non-rotating control experiment; visualization is performed with rhodamine dye. Note, that convection is confined in a region of depth $\approx \lambda$ and does not invade the region under the boundary where N is larger.

Rotation rate Ω was increased gradually before reaching its target value (in increments of $\Delta\Omega \approx 0.2$ rpm in every 5 minutes). At this point the system was left undisturbed for 30-40 minutes, thus the early transients of the rotating double-diffusive cell formation were not observed. Then, PIV measurements were conducted using horizontally illuminated laser sheets at different water depths. Two slightly different arrangements were used. For the first one, a camera together with a laser were fixed on an arm from the sidewall of the container. Close ups of the velocity fields could be acquired in this manner. In the second set-up, complete views of the velocity fields in the full annulus could be observed from a co-rotating camera platform situated above the tank (as depicted in Fig. 1). Alongside these PIV cameras, an infrared thermographic camera was also mounted on the platform to enable the simultaneous observation of the temperature field at the free water surface. At the end of the PIV measurements, rotation rate Ω was lowered gradually (in the same manner as in the spin-up phase), and after the flow reached a full stop, a second salinity profile was also recorded.

3 The Barostrat Instability

As expected, above a rotation rate threshold (see Kerr (1995)), the baroclinic instability destabilizes the flow in a shallow layer, generating a ring of vertically confined vortices. The azimuthal wavenumber m of the instability is a function of the thickness of the convective layer (itself depending on the local density stratification and on the temperature difference) and on the rotation rate Ω. Aside to infrared temperature measurements of the free surface fluid layer, Particle Image Velocimetry (PIV) measurements were also conducted using horizontally illuminated laser sheets at different water depths, which were observed from a co-rotating camera. Figure 3 shows an example of the infrared image of an azimuthal wavenumber m=4 unstable pattern superimposed with its corresponding velocity field measured closed to the surface. To our knowledge, these are the first experimental observations of these combined convective and baroclinic instabilities in a rotating stratified layer and we coin this phenomenon the "Barostrat Instability".

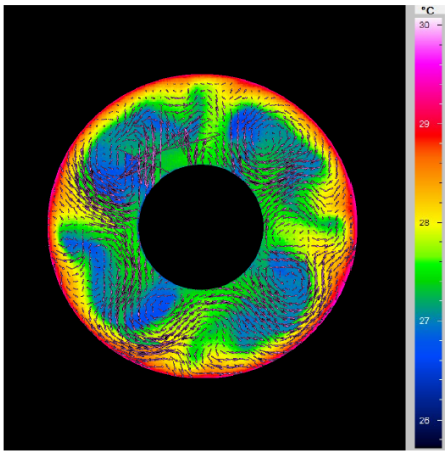

Figure 3: Infrared image superimposed with the PIV velocity field near the surface. $\Delta T = 6\ K$, $\Omega = 2.7\ rpm$.

We performed different experiments at the following values of global parameters: $\Delta T = 10$ K and $\Omega = 2$rpm (denoted as Exp. 4), $\Delta T = 9.6$K and $\Omega = 3$ rpm (Exp. 5), $\Delta T = 9$ K and $\Omega = 4$rpm (Exp. 6), $\Delta T = 9$ K and $\Omega = 5$ rpm (Exp. 7). Fig. 4 presents the vertical mean azimuthal velocity profile as measured in the experimental runs denoted Exp.4 to Exp.7, as mentioned above. For each point we calculated the mean velocity over the whole investigated horizontal plane, which corresponds to approximatively one sixth of the cylindrical gap in the azimuthal direction. Since the presence of baroclinic instability breaks the axial symmetry of the flow, temporal averaging was performed upon a sufficient timespan to permit that the flow from different segments can contribute to the final azimuthal mean (between one and 2.5 minutes). Although the vertical resolution is rather poor (9 data points in the full water layer) one can easily recognize on Fig. 4 the opposite signs of the zonal flows at the borders of the convective cells. In the small region between them only weak flow was measured. It is to be emphasized, that despite the differences in rotation rate Ω and temperature difference ΔT, all four experiments yielded very similar results. Moreover, it is possible to estimate in each case the vertical velocity gradients that should be proportional to the radial temperature gradients divided by the rotation rate Ω as predicted by the thermal wind equation. This equation expresses the geostrophic balance within the flow and our velocity and temperature gradients measures

are in fairly good agreement with this equilibrium as can be seen in Fig. 5).

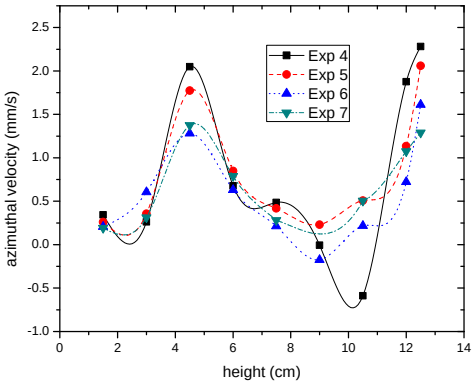

Figure 4: Vertical azimuthal velocity profile as calculated from the four experiments mentioned above. Both convective cells sustaining strong zonal flows of opposite signs at top and bottom of the whole layer are visible.

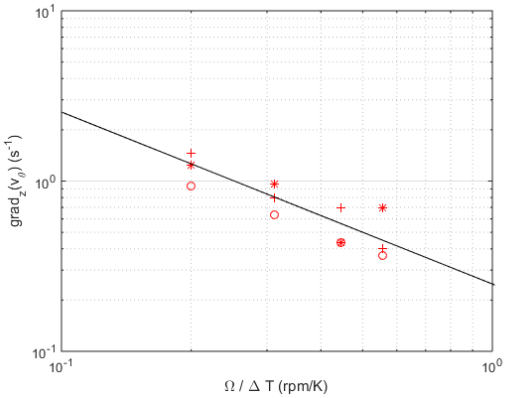

Figure 5: Verification of the geostrophic balance for the four experiments mentioned above. The geostrophic balance within the flow, as given by the thermal wind equation, is illustrated by the -1 slope line in this log-log representation.

4 Perspectives

The next question is then to explore the possible ways to escape from the geostrophic equilibrium with the generation of Internal Gravity Waves (IGWs) by the Barostrat Instability as it can be the case for instance in unbalanced dynamics of atmospheres; see for instance O'Sullivan and Dunkerton (1995) or Plougonven and Snyder (2007). For the first time Jacoby et al. Jacoby et al. (2010) looked for IGWs in a classical continuously stratified, differentially heated rotating annulus. They found signatures for high-frequency waves but surprisingly the waves were related to boundary layer instabilities and not to the fronts of baroclinic waves. Recently, Borchert et al. Borchert et al. (2014) and Randriamampianina and del Arco Randriamampianina and del Arco (2015) numerically investigated the occurrence of IGWs by the baroclinic instability. Although we cannot

prove yet that the Barostrat Instability can generically generate IGWs, Figure 6 displays at snapshot of our PIV velocity fields that exhibits a wave train whose characteristics are compatible with IGWs. The comparison between these PIV measurements of the velocity field with numerical simulations of the baroclinic instability in the atmosphere by O'Sullivan and Dunkerton (1995) is striking.

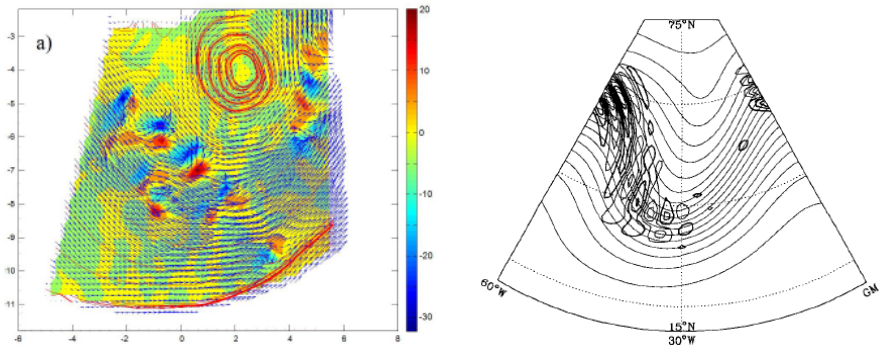

Figure 6: Comparison between experimental ($\Delta T = 10\ K$, $N = 3.3\ rad/s$ and $\Omega = 2\ rpm$) measurement of the velocity field near the surface (divergence of the field is in color) (left) and the numerical simulation of the emission of an internal wave train by the baroclinic instability in the atmosphere (from O'Sullivan and Dunkerton (1995)) (right).

References

Borchert, S., U., A., and Fruman, M. D. (2014). Gravity wave emission in an atmosphere-like configuration of the differentially heated rotating annulus experiment. *J. Fluid Mech.*, 758:287–311.

Chen, C., Briggs, D., and Wirtz, R. (1971). Stability of thermal convection in a salinity gradient due to lateral heating. *International Journal of Heat and Mass Transfer*, 14:57–62.

Jacoby, T. N. L., Read, P. L., Williams, P. D., and Young, R. M. B. (2010). Generation of inertia-gravity waves in the rotating thermal annulus by a localized boundary layer instability. *Geophys. Astrophys. Fluid Dyn.*, 105.

Kerr, O. (1995). The effect of rotation on double-diffusive convection in a laterally heated vertical slot. *J. Fluid Mech.*, 301:345–370.

O'Sullivan, D. and Dunkerton, T. (1995). Generation of inertia-gravity waves in a simulated life cycle of baroclinic instability. *J. Atmos. Sci.*, 52:3695.

Plougonven, R. and Snyder, C. (2007). Inertia-Gravity Waves Spontaneously Generated by Jets and Fronts. Part I: Different Baroclinic Life Cycles. *J. Atmos. Sci.*, 64:2502–2520.

Randriamampianina, A. and del Arco, E. C. (2015). Inertiagravity waves in a liquid-filled, differentially heated, rotating annulus. *J. Fluid Mech.*, 782:144–177.